05863-13-T

THE UNIVERSITY OF MICHIGAN

COLLEGE OF ENGINEERING
DEPARTMENT OF AEROSPACE ENGINEERING
HIGH ALTITUDE ENGINEERING LABORATORY

Technical Report

Earth Reflectance Patterns Measured by Radiometer on High Altitude Balloon Flights

F. L. BARTMAN

Under contract with:

National Aeronautics and Space Administration
Contract No. NASr-54(03)
Washington, D. C.

Administered through:

December, 1968

OFFICE OF RESEARCH ADMINISTRATION • ANN ARBOR

THE UNIVERSITY OF MICHIGAN

COLLEGE OF ENGINEERING

Department of Aerospace Engineering
High Altitude Engineering Laboratory

Technical Report

EARTH REFLECTANCE PATTERNS MEASURED BY RADIOMETER ON HIGH ALTITUDE BALLOON FLIGHTS

Fred L. Bartman

ORA Project 05863

under contract with:

NATIONAL AERONAUTICS AND SPACE ADMINISTRATION

CONTRACT NO. NASr-54(03)

WASHINGTON, D. C.

administered through:

OFFICE OF RESEARCH ADMINISTRATION ANN ARBOR

December, 1968

This report is the text of a paper presented at the International Colloqium on the utilization of Balloons for Scientific Research held at the Centre National d'etudes Spatiales, Paris, France, 10-13 July, 1967.

ACKNOWLEDGEMENTS

The help of all my colleagues in the High Altitude Engineering Laboratory in carrying out preparations and field operations for the balloon flight measurements is also acknowledged. Of these, the work of Mr. Michael Surh, on radiometer calibration, and Messers. Leo W. Carls, Paul A. Titus, Wan Y. Lee, and David Hartsig on field operations and radiometer data processing is particularly appreciated.

The financial support received from the National Aeronautics and Space Administration under Contract NASr-54(03) is also gratefully acknowledged. Numerous discussions of radiometer calibrations and the manner of interpretation of radiometer data with Dr. William Nordberg, Mr. William Bandeen and other members of the staff of Goddard Space Flight Center, and of Mr. Frank Malinowski of Santa Barbara Research Corporation have also been very helpful.

TABLE OF CONTENTS

List of Figures

EARTH REFLECTANCE PATTERNS MEASURED BY RADIOMETER ON HIGH ALTITUDE BALLOON FLIGHTS

ABSTRACT

Earth reflectance patterns for 0.55 to 0.75 micron and 0.2 to 5.0 micron solar radiation, measured by radiometer from balloons at 32 to 34 km, are presented and compared with theoretical patterns and other experimental data. The data indicate the spectral dependence and non-isotropic nature of the earth's reflectance. The balloon gondola and instrumentation are described.

1. INTRODUCTION

Radiometers of the same type as the five channel radiometers flown on the TIROS and NIMBUS satellites have been flown on a series of high altitude balloon flights by members of the University of Michigan's High Altitude Engineering Laboratory, as a part of a research and development program in support of the NASA Goddard Space Flight Center's Meteorological Satellite Program.

The data that will be presented was obtained on three balloon flights. The dates of these flights and the radiometers used for the measurements are:

2 June 1962	TIROS #103A Five - Channel Radiometer
26 June 1963	TIROS #103A Five - Channel Radiometer and NIMBUS #F1 MRIR Radiometer
10 March 1965	NIMBUS F-4 MRIR Radiometer

2. EARTH REFLECTANCE

2.1 The Nature of Scattering and Reflection by the Earth

The geometry of scattering and reflection is illustrated by Figure 1. Q is the point at which reflection or scattering takes place. SQ is the ray from the radiation source; in this case, the sun. QR is the reflected or scattered ray. The plane SQZ is called the principal plane and the plane SQR is called the scattering plane. The incident ray is defined by the polar coordinates (θ_o, ϕ_o), where θ_o is the zenith angle and ϕ_o the azimuth angle measured counterclockwise from the north direction to the extended principal plane. The reflected or scattered ray is measured by its polar coordinates (θ, ϕ). The angle Ψ is equal to $\phi - \phi_o$. β is the scattering angle.

The reflectance in the direction (θ, ϕ) for an incident ray (θ_o, ϕ_o) is called the bi-directional reflectance:

$$\rho(\theta_o, \phi_o, \theta, \phi)$$

The total reflectance over the hemisphere is called the directional reflectance:

$$r(\theta_o, \phi_o) = \frac{1}{\pi} \int_{\phi=0}^{2\pi} \int_{\theta=0}^{2\pi} \rho(\theta_o, \phi_o \theta, \phi) \cos\theta \sin\theta \, d\theta \, d\phi$$

A schematic diagram illustrating the measurement of cloud reflectance is shown in Figure 2. Radiation scattered back up to the radiometer by the cloud is measured as desired. In addition, scattered radiation from the air above and below the cloud, and some radiation reflected back upward by the earth will be measured by the radiometer. The reflectance measured will be a function of the cloud's physical characteristics; its thickness, height above the ground, absorption of the cloud particles, liquid water content and the particle size distribution. In addition the reflectance will depend on the incidence and reflectance angles and the reflectance of the surface below the cloud.

Theoretical calculations which consider all of these effects have not yet been made. Recent published results of interest include the following. Diermendjian[1] has derived scattering patterns for single scattering from a water cloud with realisitc size distribution, i. e. for scattering from a small volume element of a cloud. Twomey, Jacobwitz and Howell[2] have obtained results for multiple scattering in clouds. These calculations include the effects of cloud thickness, absorption, drop size distribution, liquid water content, and directions of the incident and emerging radiation. Scattering by air molecules above and below the cloud and surface reflectance were not considered.

Other experimental results of cloud reflectance measurements have been reported on by Salmonson, [3] and Cherrix and Sparkman, [4] the former were made from an aircraft flying 300 meters above the clouds over the ocean and the latter from an aircraft flying at 12 kilometers over clouds above both ocean and land.

The balloon flight data on cloud reflectance will be compared with the above noted theoretical and experimental results.

2.2 Interpretation of the Radiometer Data

The values of reflectance measured by the visible channels of the medium resolution radiometers differ from the actual earth reflectances which we desire to measure, as follows. Assuming normal incidence, we want to measure:

$$\rho = \frac{\frac{1}{\pi}\int_0^\infty \rho_\lambda H_{s\lambda}\, d\lambda}{\frac{1}{\pi}\int_0^\infty H_{s\lambda}\, d\lambda}$$

where ρ_λ is the spectral bi-directional reflectance $H_{s\lambda}$ is the spectral solar irradiance.

We actually measure:

$$\rho' = \frac{\frac{1}{\pi}\int_0^\infty \rho_\lambda H_{s\lambda}\, \phi_\lambda\, d\lambda}{\frac{1}{\pi}\int_0^\infty H_{s\lambda}\, \phi_\lambda\, d\lambda}$$

where ϕ_λ is the spectral response function of the instrument.

Thus, in addition to calibration errors, we have the error in interpretation due to the fact that we have measured a weighted average reflectance using the weighting function $H_{s\lambda}\,\phi_\lambda$ instead of $H_{s\lambda}$.

Weighting functions for the visible channels of the TIROS #103A five channel radiometer are shown in Figures 3 and 4. The weighting function for the wide band channel (Figure 3) is similar to the function $H_{s\lambda}$. The weighting function of the NIMBUS F-4 MRIR places relatively greater emphasis on the $\lambda > 1$ micron region. The weighting function of the narrow band channel (Figure 4) emphasizes the spectral range of 0.55 to 0.75 micron, especially the 0.58-0.60 micron region. It is apparent that the reflectances measured with the narrow band channel cannot necessarily be interpreted as total reflectances over the 0.2-4.0 micron range.

It is important to keep in mind that the quantity measured is a bi-directional reflectance. The assumption that the surface is a diffuse reflector will often lead to error. It is absolutely necessary to make measurements at all angles of incidence and reflectance to correctly evaluate reflectance data.

3. The Balloon Flight Measurement System

Figure 5 is a photograph of the balloon gondola used on the 2 June 1962 balloon flight, shown suspended from the back of the launching truck. The TIROS five-channel radiometer projects from the balloon gondola on the left and a 70mm aerial camera, boresighted with the radiometer, is on the right. Another 70mm camera, looking vertically downward, is in the front of the gondola.

The TIROS radiometer and its associated camera were mounted on the ends of a horizontal shaft. When the shaft was rotated, the field of view of the radiometer and camera moved in a conical scan (60^{o} cone half angle) across the surface of the earth from horizon to horizon.

At the top of the gondola was a circular ring with a set of photocells for the measurement of the azimuth of the shaft with respect to the sun. The sun's azimuth and elevation are known accurately as a function of time.

The geometry of the radiation measurements is exactly that shown in Figure 1, so that when measurements are made, information about bi-directional reflectance patterns, or scattering patterns, is obtained.

The instrument arrangements for the other balloon flights was similar to that shown in Figure 5. When the NIMBUS MRIR was used, it was mounted on the gondola in such a fashion that, with a motionless gondola, it would scan the earth from horizon to horizon, in a vertical plane. When the gondola rotates, its azimuth data must be considered in the calculation of reflectance and scattering patterns.

The balloon gondola does not hang vertically beneath the balloon during the ascent portion of the flight. However as it approaches its float altitude and begins to move with the wind, it assumes a position vertically beneath the balloon and a well defined coordinate system is obtained.

An FM-FM telemetry system was used to transmit data to a mobile telemetry ground station. The airborne portion of the system consists of up to about 12 voltage controlled oscillators, a mixing amplifier, a two watt transmitter and a crossed dipole antenna system. The telemetry ground station is built into a bus (see figure 6). Antennas and a preamplifier are located on the roof of the bus, and receivers, FM discriminators, direct writing recorders, tape recorders, A-D conversion equipment with paper tape punch and flexowriter print out, WWV receiver, standard time code generator, and a small solid state digital computer are located inside of the bus.

The airborne antenna is mounted in a horizontal plane, beneath a horizontal reflector, under the balloon gondola and radiates quite uniformly in all directions below and to the side of the balloon gondola. The maximum range of the telemetry is determined by the horizon as viewed from the gondola. When the balloon is at 35 km altitude, the horizon is about 685 km away. With the ground station built into a bus, the length of a flight, for which data can be received, is increased by moving the bus along the road in the same direction as the balloon is traveling. Data can be received and recorded without difficulty as the bus moves over modern roads at speeds up to 80 km per hour. When the bus is moving, a corner reflector, steerable in azimuth from inside the bus, is used. When the bus is standing still, a bilfilar helical antennae can be used on top of the bus.

The accuracy of the telemetry system is about 0.5% of full scale for low frequency signals of the radiometer type. This accuracy is checked and maintained by two independent 5-point calibration units with which the telemetry system is calibrated at 5-minute intervals before, after, and throughout the flight. This 0.5 accuracy in the telemetry is better than the accuracy of calibration of the radiometer and thus does not significantly limit the data accuracy.

4. REFLECTANCE OF CLOUD COVERED EARTH

4.1 Reflectance Data

The 2 June 1962 balloon flight was launched through a layer of low altitude clouds at 1034 GMT (0434 CST), from Sioux Falls, S. D. (43.4^{o}N-96.7^{o}W). It floated at an average altitude of 113000 feet (34km) for about 13 hours above various types of cloud cover, as follows (see figure 7).

Time, GMT	Cloud Type	Sun's Elevation Degree
1034-1300	Stratocumulous, 1000-2000 ft. thick tops at about 4500-6000 feet.	0-22
1300-1745	Cirrus above stratocumulous	22-68
1745-2000	Broken cumulus	68-56
2000-0100	Cirrus above scattered cumulus	56-10

The reflectance data obtained is difficult to analyze when the clouds viewed are nonhomogeneous as in the last three cases. It is only when the cloud surface is quite uniform and homogeneous, as it was up to 1300 GMT; so that the radiometer field of view is completely filled by the same type of cloud surface, that the data is well enough defined to plot a scattering pattern. At the same time,

the gondola motion is azimuth combined with the conical scan of the radiometer must be such that data covering a wide range of scattering angles is obtained. Such data was obtained in four 40-sec intervals at 1157, 1215, 1233, and 1251 GMT. Even then, it was necessary to eliminate portions of the data obtained when wispy cirrus or shadows of wispy cirrus came into the field of view. This data, plotted as a function of the scattering angle β, is shown in Figure 8 for the 0.2-5.5 micron channel of the radiometer.

Data was obtained for scattering angles, β, of 50-145°. There are maxima of scattering at low scattering angles and at high scattering angles, with a minimum at β equal to 110-120°. There are indications of a fogbow (a maximum) at about 135°. There is a certain amount of scatter in the data, which is probably due to nonuniformities in the cloud structure (i.e., composition and thickness).

There is an indication of a slight increase in forward scattering and a slight decrease in backscattering with increasing time(i.e., increasing sun elevation angle). However, because of insufficient knowledge about the exact cloud thickness and physical characteristics during the time interval involved, it is not certain that the increase in forward scattering and decrease in backscattering is caused by the increase in sun elevation angle.

4.2 Comparions with Single Scattering Theory

Smoothed curves for each of the channels were essentially the same within the accuracy of the radiometer measurements, so that it is reasonable to take an average as representative of the scattering pattern of stratocumulus clouds, over South Dakota farmland, 300-600 meters thick with tops at about 1400-1800 meters. This average of the radiometer data for stratocumulus clouds is shown in Figure 9 with Deirmendjian's[1] calculation for single scattering in a water cloud model for comparison. For this comparison, the experimental

curve has been normalized to unity, just as Deirmendjian's curve is, that is, the integral over the 4π solid angle is unity for each curve. While the single scattering model does not produce the intensity of the actual cloud scattering, the qualitative agreement of the functional relationship should be noted, even to the existence of the maximum of the curve at $\beta=136^{o}$ (i. e., the fogbow). This angle is less than the theoretical angle of 143^{o} for $\lambda = 0.70$.

Since data was obtained only for $50^{o} < \beta < 145^{o}$ the experimental curve has been extrapolated from 50^{o} to 0^{o} and from 145^{o} to 180^{o} using the theoretical curve as a guide. This final curve, is a final estimate of the scattering pattern of a stratocumulous cloud. A three-dimensional model of this scattering pattern is shown in Figure 10. In this figure, the flat circular disk represents the top of a flat cloud. Solar radiation is incident from the right at an elevation angle of 20^{o}. The spike in the scattering pattern pointing to the right is backscattering. The fogbow is the next "scallop" in the pattern. The large amount of forward scattering is shown at the left. The truncation of this forward scattering is merely due to the limit in the size of the model. The small bow in the center of the pattern may possibly be due to noise. Deirmendjian's calculations show that such a bow exists at 5. 3 microns but not at lower wavelengths.

4. 3 Comparison with other Experimental Data

In figure 11 the narrow band channel data is compared with measurements reported by Salomonson[3] and G. T. Cherrix and B. A. Sparkman.[4]

Salomonson's data was taken from 300 meters above stratus clouds over the Pacific Ocean near San Francisco, California. Cloud thickness was about 330 meters with cloud tops at 550 meters. The solar zenith angle was $62\text{-}67^{o}$. Measurements by Salomonson at other zenith angles differ somewhat from the ones shown in this figure. For zenith angles of slightly lower altitude, he obtained slightly higher reflectance for $80 \leq \beta < 150$ degrees. On the first day, with zentih

angles of 12-13 degrees, with a somewhat thinner and lower cloud, he obtained smaller values of reflectance for $\beta < 120^{o}$.

The data of Cherrix and Sparkman shown here for comparison were taken from an altitude of 12 kilometers above stratocumulus over the O'Keefenokee swamp in southern Georgia. The solar zenith angle was 73^{o}, cloud tops were estimated to be at 1700-1900 meters. Cloud thickness is not known. Data taken at other zenith angles, $66\text{-}69^{o}$, showed higher reflectance for $90 < \beta < 140^{o}$.

The three sets of data show qualitative agreement. Salomonson's data do not show a fogbow at 140^{o}. This may be due to the fact that for his measurements the solar zenith angle was $62\text{-}67^{o}$, whereas the portion of the balloon measurements which indicates the fogbow were taken with solar zenith angles of $76.5\text{-}80^{o}$.

A result of the theoretical calculations of Twomey, Jacobowitz and Howell[2] may be reconciled with the fogbow obtained on the balloon flight data for zenith angles of $76.5\text{-}80^{o}$, when none were obtained by Salomonson or Cherrix and Sparkman at zenith angles up to 67^{o}. Twomey et al. have calculated the ratio of singly scattered radiation to multiply scattered radiation. They find, that in general, a large amount of singly scattered radiation is obtained only for the most tenuous clouds. However when the solar zenith angle and the reflectance zenith angles are both very large an appreciable amount of singly scattered radiation may be obtained (10% or larger). These are precisely the conditions under which the 2 June 1962 balloon flight data were obtained.

4.4 Comparison with Multiple Scattering Theory

In Figure 12 the narrow band results are compared with the theoretical results obtained by Twomey, Jacobowitz and Howell[2] for multiple scattering.

Balloon flight data taken with solar zentih angle of 78.5^{o}, radiometer zenith angle of 60^{o} and azimuth varying from $1\text{-}141^{o}$ are compared with theoretical data for solar zenith angles of 75.5^{o} and 81.4^{o} and a scattering zenith angle of 63.3^{o}. The cloud model used by Twomey et al. for the theoretical multiple scattering data had a Gaussian particle size distribution with average radius of 6 microns and standard deviation of 1 micron. Other important parameters were $\lambda = 0.76$ microns, a liquid water content of 0.30 gm/m^{-3}, an extinction coefficient of 73.11 km^{-1} with zero absorption and a cloud optical thickness, $\tau = 67.1$ which would correspond to a geometrical cloud thickness of 918 meters.

The experimental and theoretical data show only rough qualitative agreement. The experimental data show almost twice as much reflectance at $\Psi = 90^{o}$, as the theoretical results predict. This disagreement may be due to one or both of the following reasons:

1) Surface reflectance and scattering by air molecules is neglected in the calculations.

2) The cloud particle size distribution may differ from that used for the theoretical data.

5. THE WAVELENGTH DEPENDENCE OF EARTH REFLECTANCE

Radiometer measurements taken simultaneously by the two channels of the radio-meter on this flight and by both the TIROS and NIMBUS radiometers on a balloon flight on 26 June 1963 are shown in Figure 13. The ratio of the bi-directional reflectance of the wide band channel, ρ_3 divided by the bi-directional reflectance of the narrow band channel, ρ_5 is plotted vs ρ_5.

The data samples were taken at 4.5-minute intervals throughout the day, so that the diagram shows samples of data taken at different scattering angles

and for different cloud conditions. The diagram shows that for the most part channel 3 (0.2-5.5 microns) reflectances are greater than channel 5 (0.55-0.75 mciron) reflectances, with the ratio being approximately equal to 1 at high reflectances and as high as 2 for low values of reflectance.

The experimental data has been supplemented with theoretically calculated data points obtained from selected spectral reflectance curves of various types by calculating the predicted instrument measured reflectances for the spectral response regions of the two channels of the F-1 MRIR radiometer. The results are shown along with all three experimental curves in Figure 13. The calculated data are in agreement with the curves measured by the radiometers.

It is quite clear that the spectral dependence of the reflected solar radiation varies considerably with the scene viewed, and that measurements with the radiometer narrow band channel (0.55-0.86 micron) cannot be used for earth albedo without the application of a correction factor.

6. THE REFLECTANCE OF PARTIALLY SNOW COVERED EARTH

The 10 March 1965 balloon flight was launched at 1210 GMT (0610 CST) from Sioux Falls, S. D., and floated at an altituded of 32.6 kilometers for about 7 hours above terrain which was 25-90% covered with wind blown snow.

The MRIR F-4 radiometer which was flown on this balloon flight had only one channel (0.2-4.0 microns) for reasurement of reflected and scattered solar radiation. Thus reflectance ratio was not studied, however, bi-directional reflectance patterns for this type of terrain and atmosphere were obtained at three different sun zenith angles, 72^{o}, 58^{o}, and 50^{o}, at 0834, 0900, and 1110 CST, respectively. When the sun was at zenith angle greater than 72^{o}, the balloon was not yet at altitude and so data was not obtained. The reflectance patterns obtained show the sum of reflected radiance from the snow covered terrain plus the scattered radiance from the atmosphere.

Figure 14 shows a photograph of a three dimensional model of a reflectance pattern obtained at 0832-0836 CST, with the sun at a zenith angle of 72.2-71.5^{o}. The balloon was still rising, and the pressure altitude varied from 20-16.5 mb during the data taking time interval. The arrow indicates the direction of the incident radiation. The figure shows a large amount of back-scattering and even larger forward scattering. In directions approaching the zenith, the reflectance is generally diffuse.

The total directional reflectance for this pattern has been calculated. A value of 35% was obtained.

The bi-directional reflectance pattern obtained at 0855-0909 CST on this balloon flight is shown in Figure 15. The sun was approximately 5^{o} higher, i.e., at 68.3-66.0^{o} zenith angle. Inspection of the figure shows a pattern similar to that obtained at the earlier time. However, now the backscattering is less intense, but covers a slightly broader range of angles. The forward scattering is less intense and not as broad in angular range. The directional reflectance, obtained by numerical integration of this data was 36.2%, which is in agreement with the earlier value within the experimental error of measurements.

Figure 16 shows the bi-directional reflectance pattern with a much higher sun, i.e., a zenith angle of 50^{o}. The pattern is significantly different from that obtained earlier in the day. The high intensity forward and back-scattering is now a feature at this high sun angle. There is a small peak at the proper angle for backscattering and a general maximum at almost all azimuths near the horizon. There is another peak at a zenith angle about 8^{o}

greater than that for specular reflection. This is consistent with surface measurements of the mirror component of reflection from snow. The directional reflectance, obtained by numerical integration of this reflectance pattern, was found to be 30.1%, about 5% lower than the values obtained earlier in the day.

7. CONCLUSIONS

Data obtained from outside the earth's atmosphere on three high altitude balloon flights indicate both the spectral dependence and non-isotropic nature of earth reflectance. Additional measurements of this type should be made over other earth surface features.

BIBLIOGRAPHY

1. Deirmendjian, D., Scattering and Polarization Properties of Water Clouds and Haze in the Visible and Infrared, Applied Optics, 3, pp. 187-196, No. 2, February 1964.

2. Twomey, S., Jacobowitz, H., and Howell, H. B., Light Scattering by Cloud Layers, Journal of Atmospheric Sciences 24, pp. 70-79, No. 1, January 1967.

3. Salomonson, V. V., Anisotropy of Reflected Solar Radiation from Various Surfaces as Measured with an Aircraft-Mounted Radiometer, Proceedings of the Fourth Symposium on Remote Sensing of Environment, pp. 393-407, 12-14 April, 1966, The University of Michigan, Ann Arbor, Michigan.

4. Cherrix, G. T., and Sparkman, B. A., A Preliminary Report on Bi-directional Reflectances of Stratocumulus Clouds Measured with an Airborne Medium Resolution Radiometer, Report X-622-67-48, NASA Goddard Space Flight Center, Greenbelt, Maryland, February 1967.

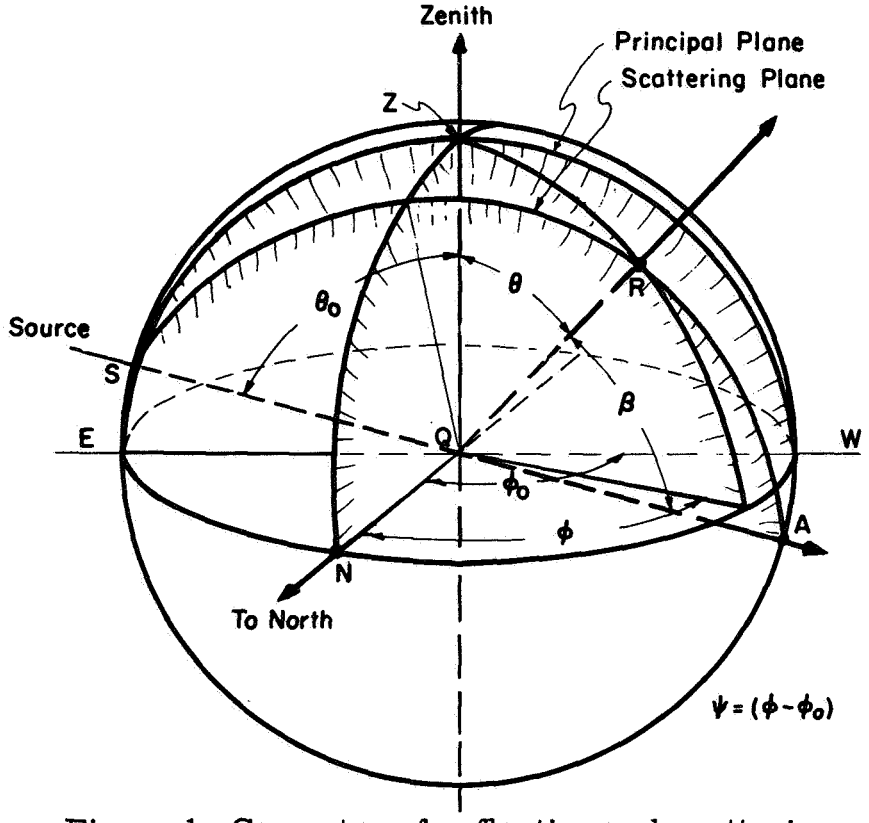

Figure 1. Geometry of reflection and scattering

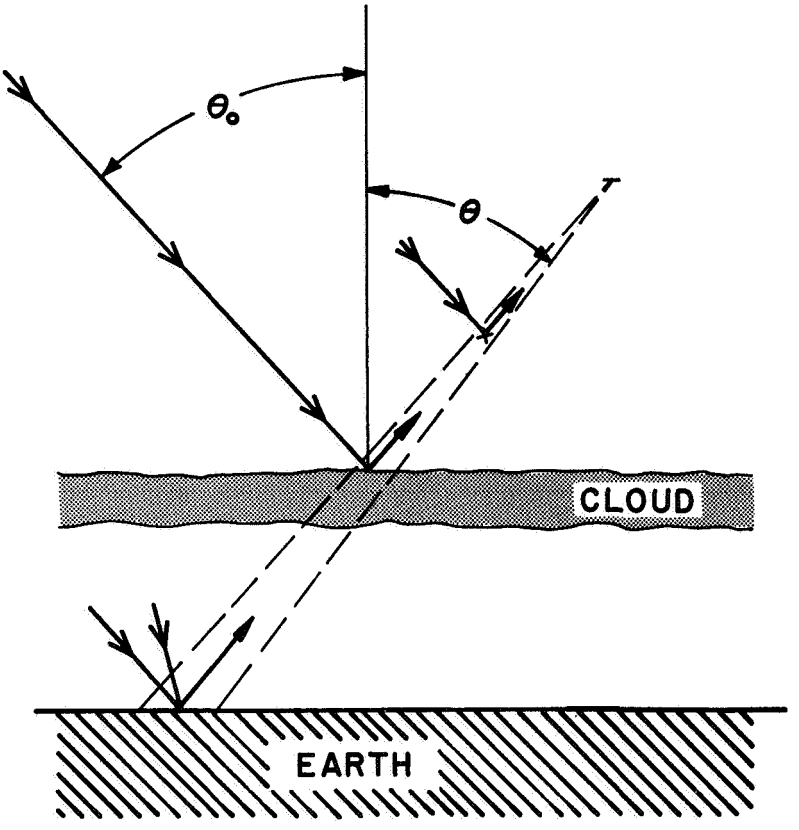

Figure 2. Schematic diagram illustrating cloud reflection

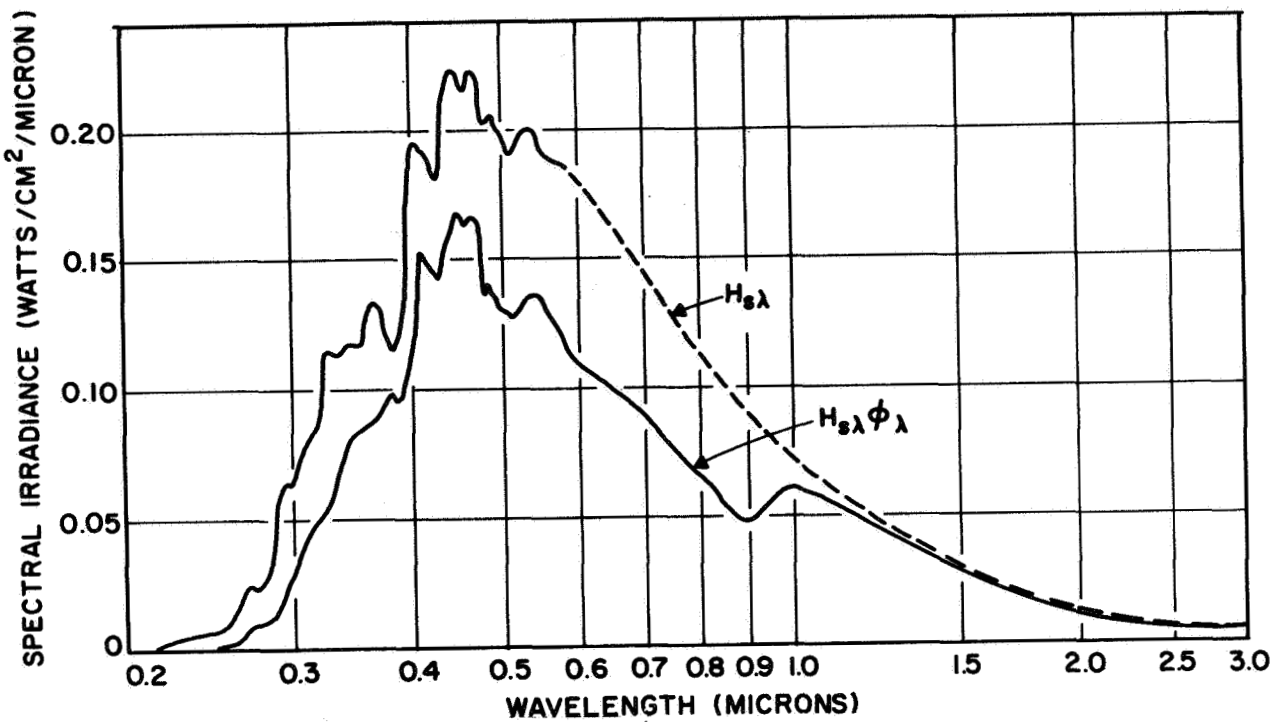

Figure 3. Weighting function, $H_{s\lambda}\,\phi_{\lambda}$ for 0.2-6.0 micron channel of TIROS 103A radiometer

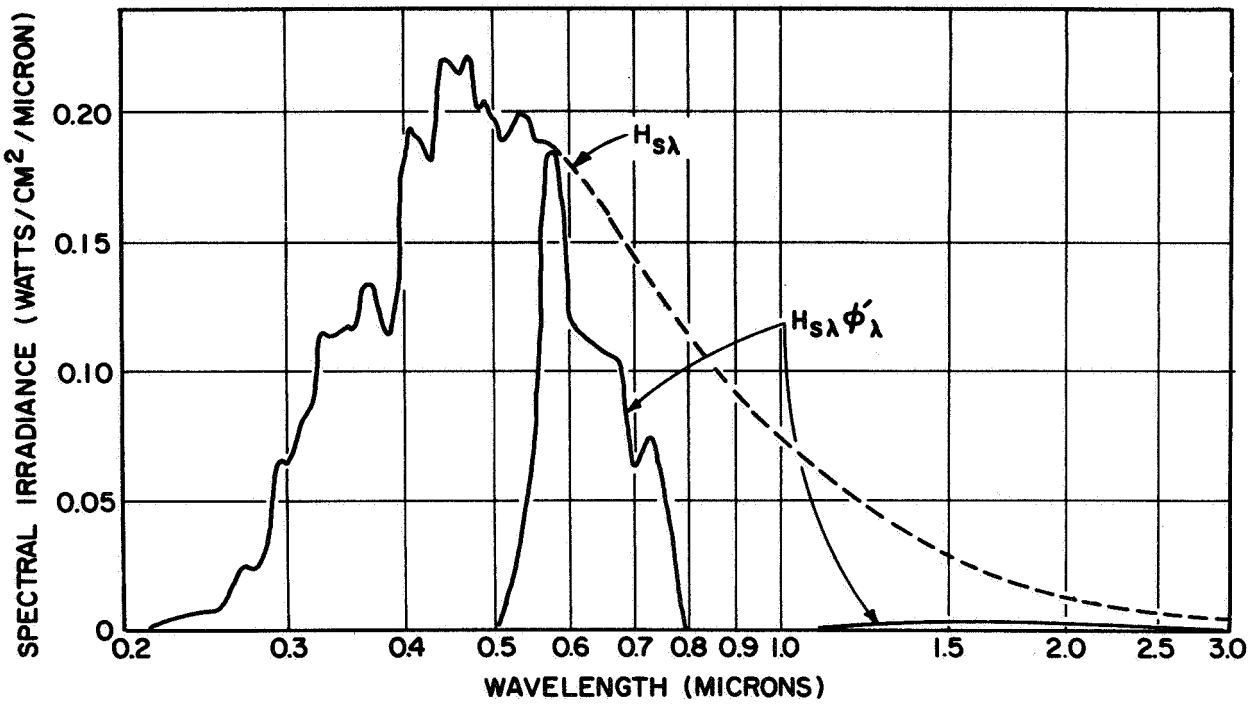

Figure 4. Weighting function, $H_{s\lambda}\ \phi_{\lambda}$ for 0.55-0.75 micron channel of TIROS #103A radiometer.

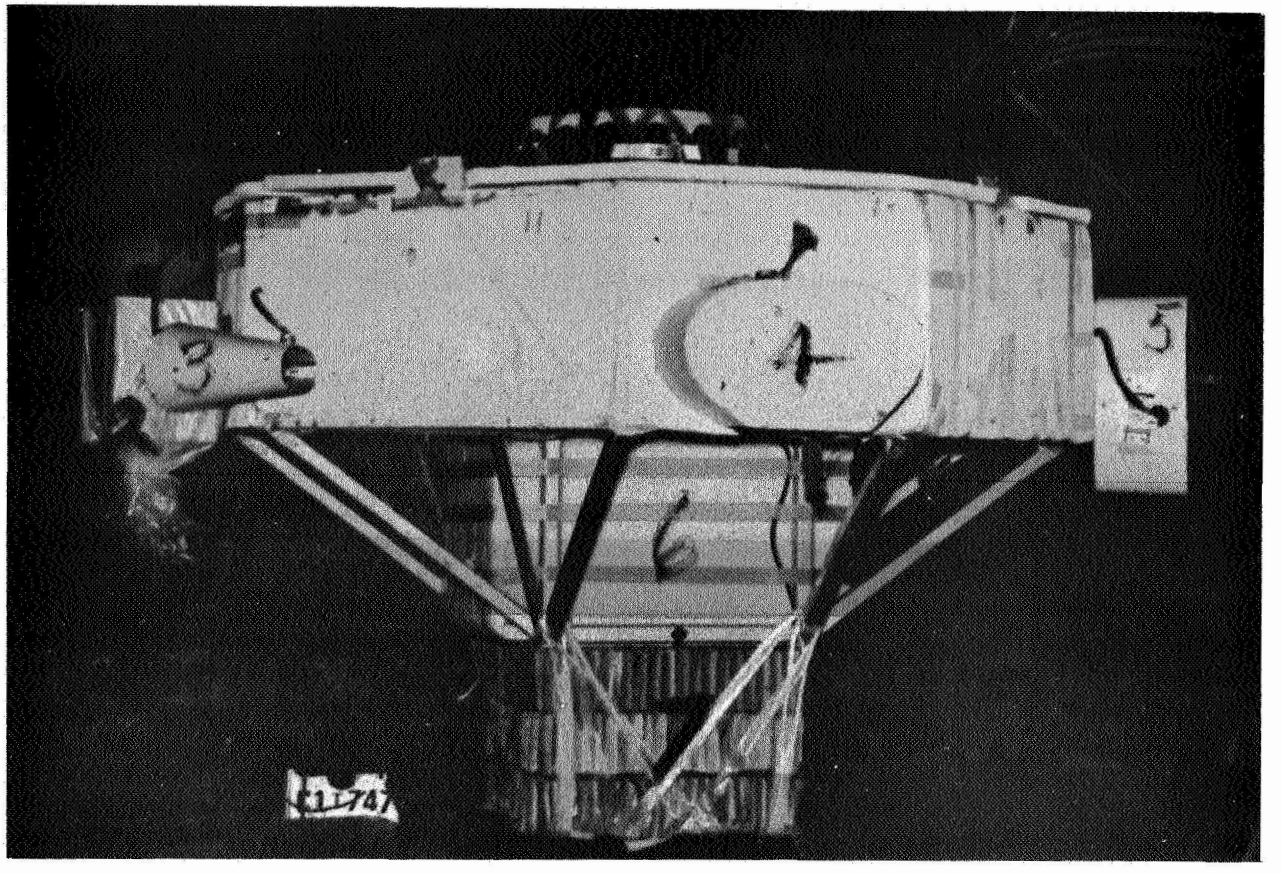

Figure 5. Balloon gondola

Figure 6. Mobile telemetry ground station

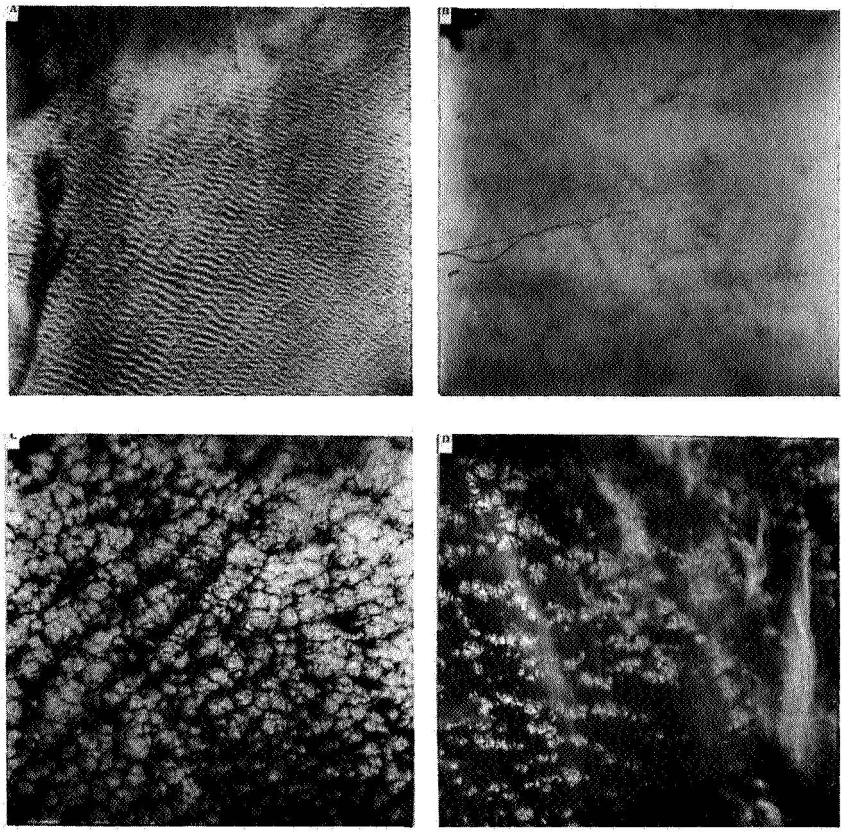

Figure 7. Photographs of cloud cover for 2 June, 1962 balloon flight

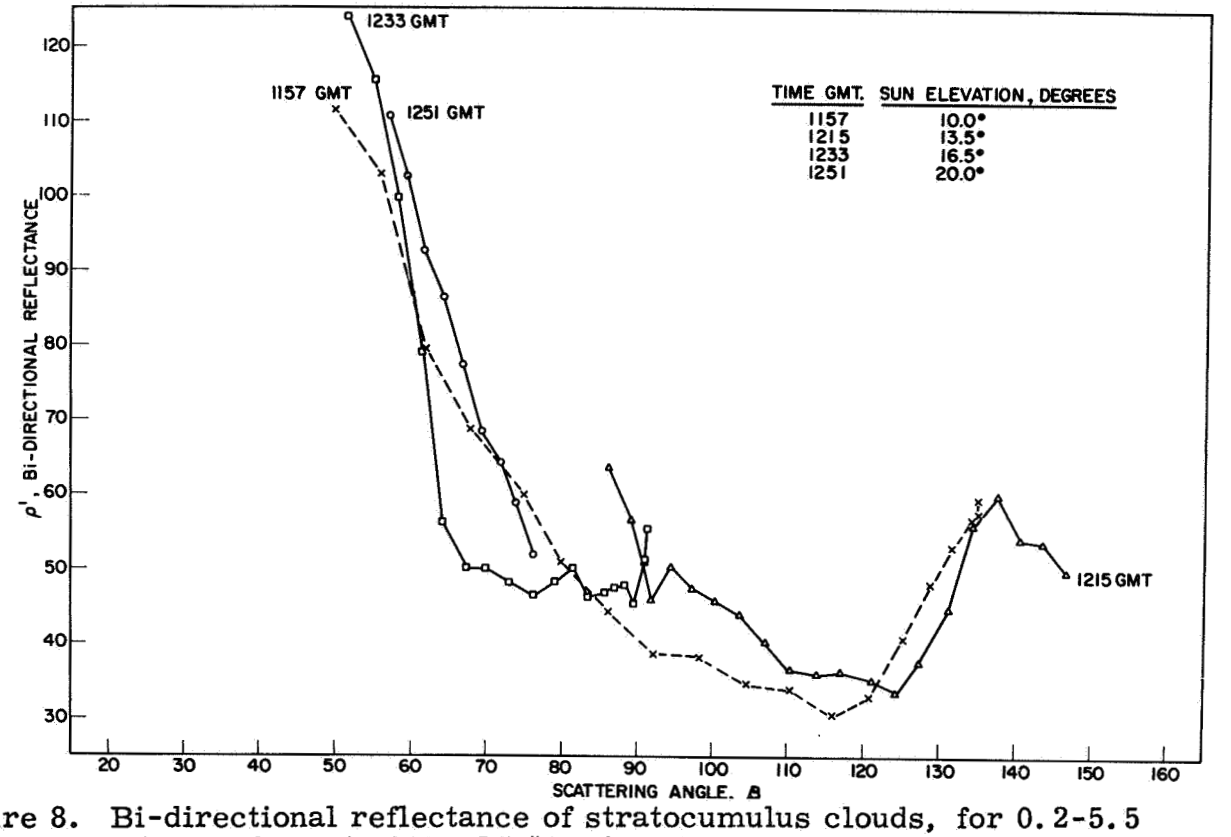

Figure 8. Bi-directional reflectance of stratocumulus clouds, for 0.2-5.5 micron channel of TIROS #103A radiometer, 2 June, 1962 balloon flight

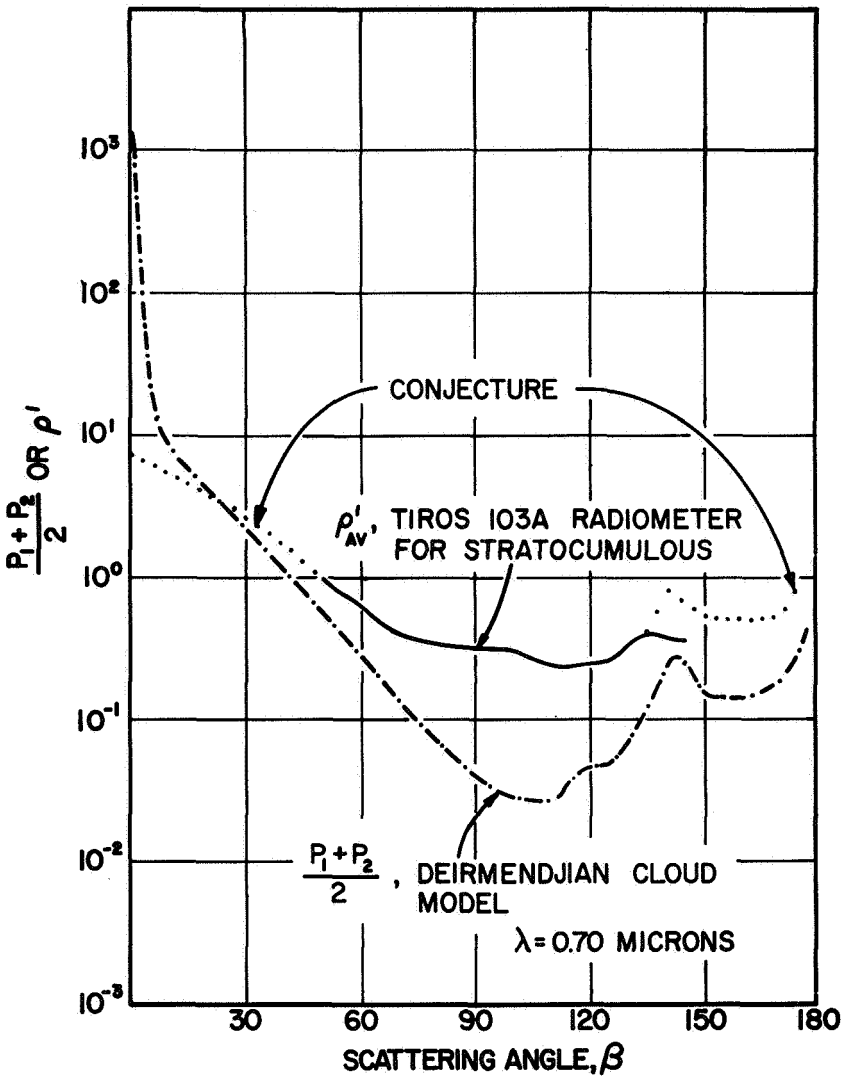

Figure 9. Comparison of experimental data on bi-directional reflectance of stratocumulus cloud with theoretical single scattering pattern of water cloud model

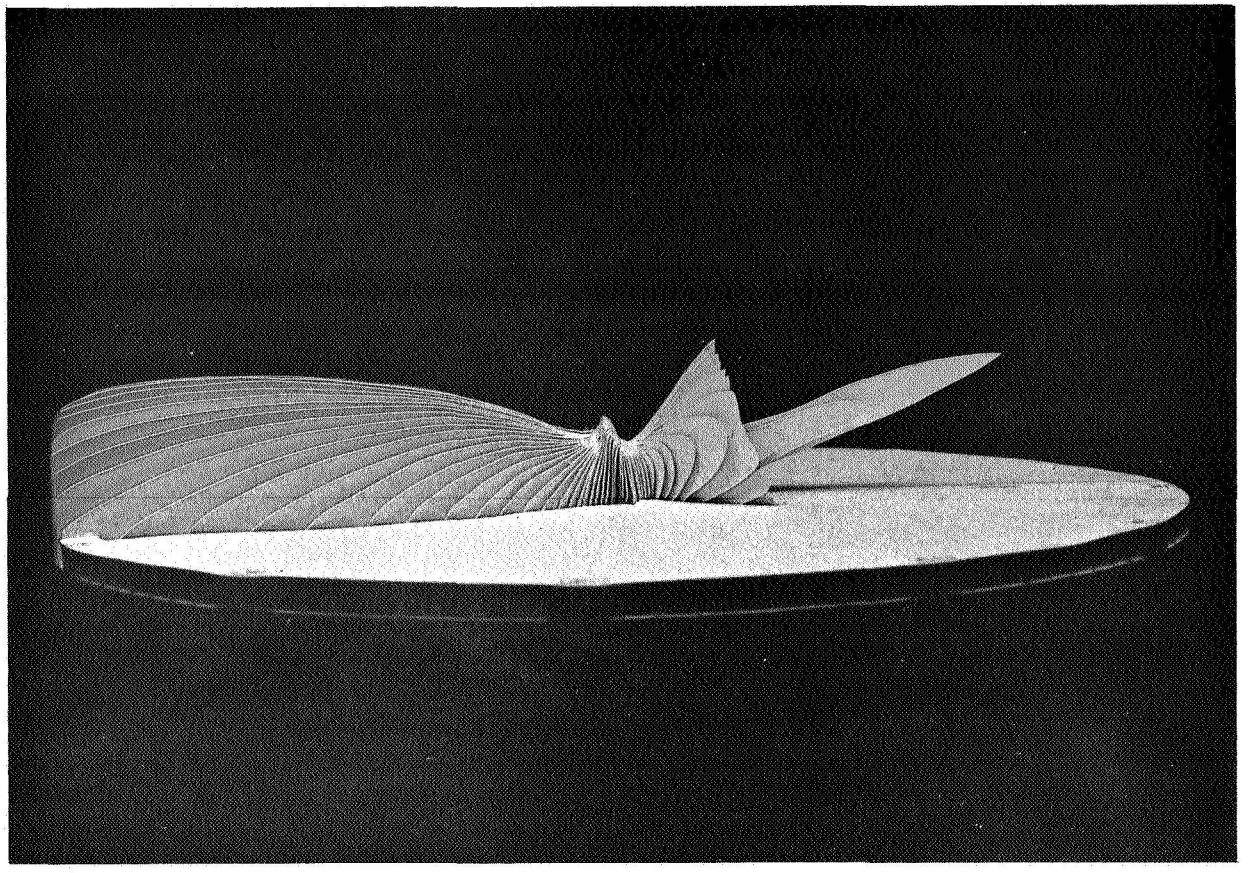

Figure 10. Model of bi-directional reflectance pattern of stratocumulus cloud

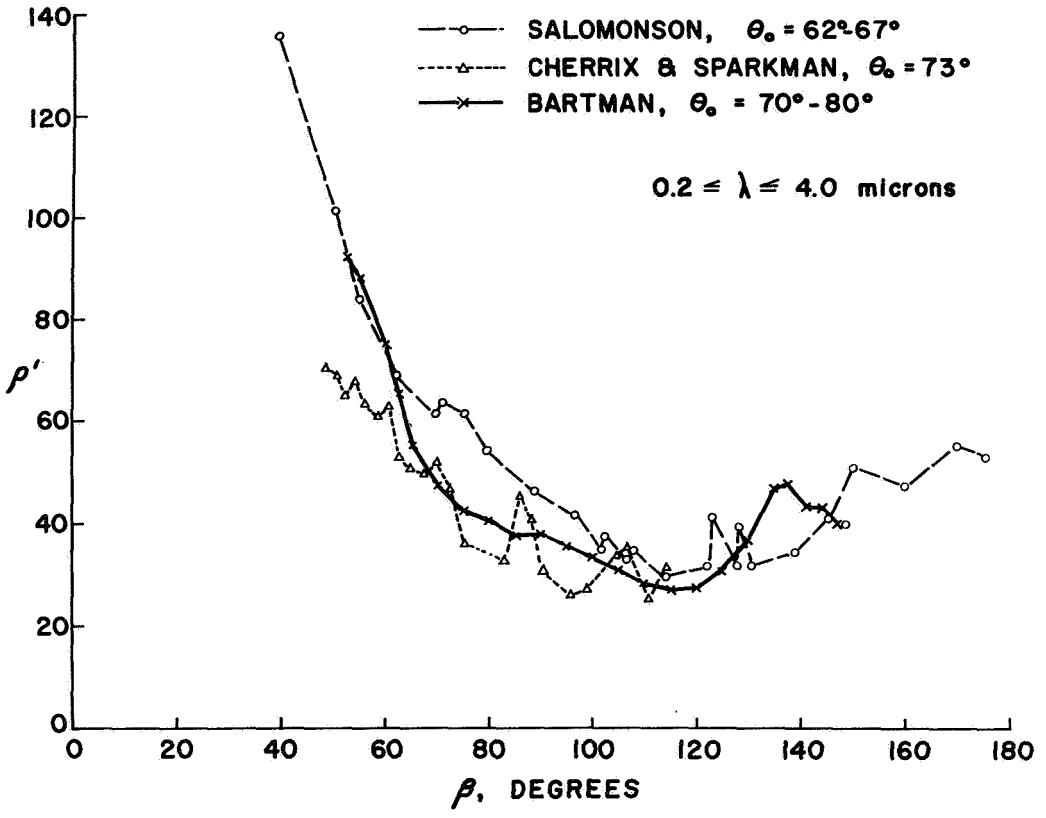

Figure 11. Comparison of experimental cloud reflectance data

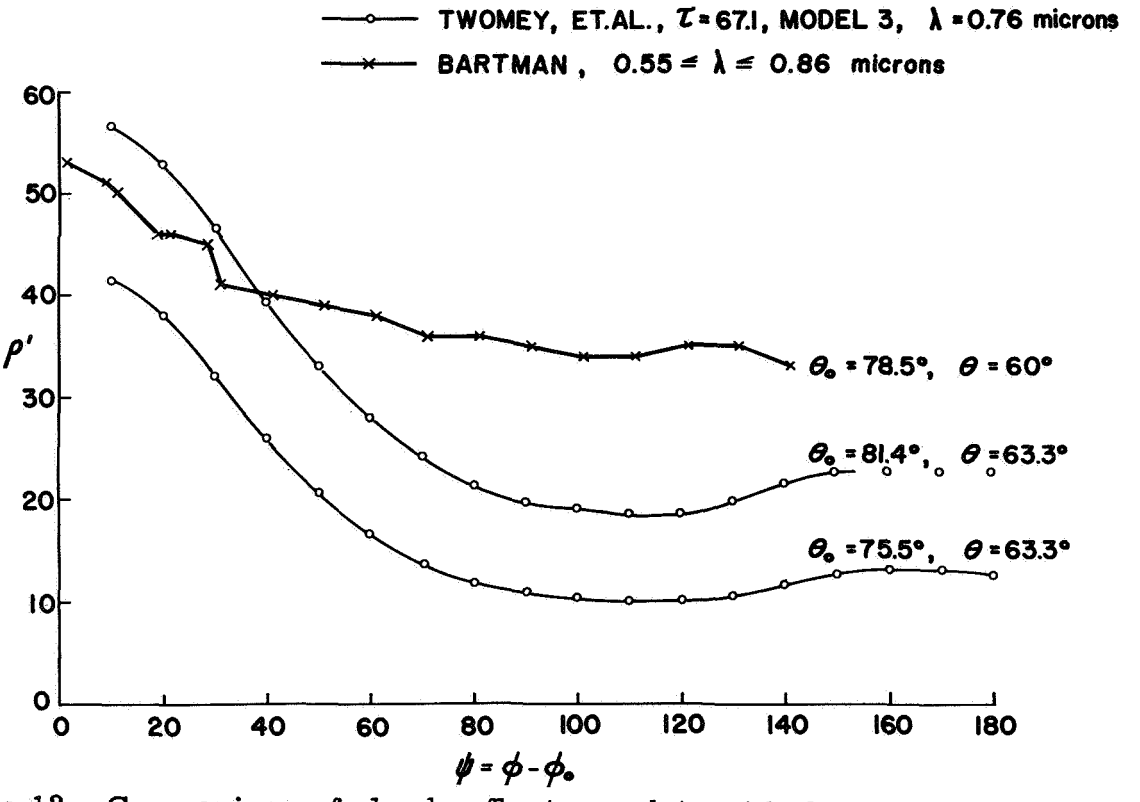

Figure 12. Comparison of cloud reflectance data with theoretical calculations of Twomey, Jacobowitz and Howell.

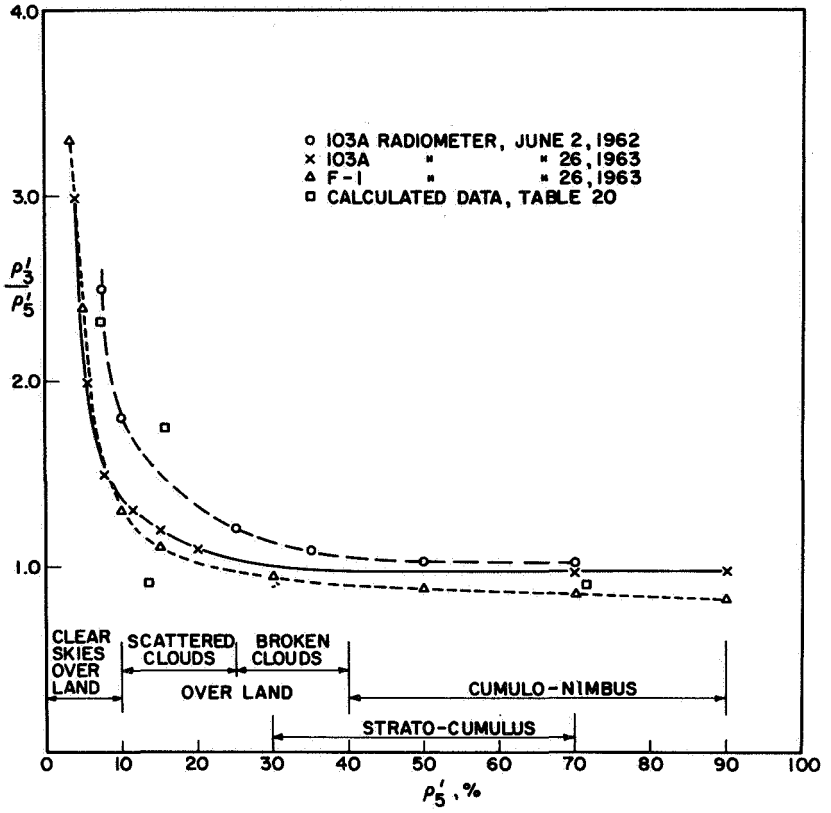

Figure 13. Reflectance diagram demonstrating spectral dependence of earth reflectance.

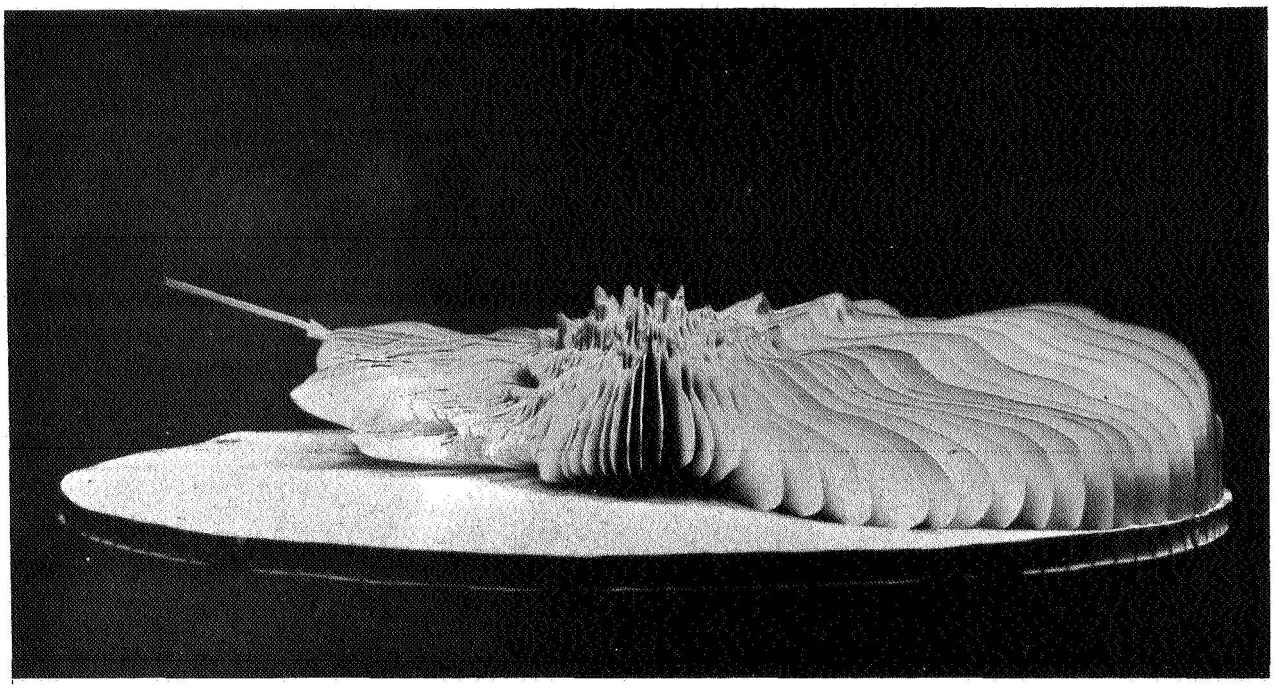

Figure 14. Photos of model of 0832-0836 CST bi-directional reflectance pattern. $\theta_o = 72.2\text{-}71.5^{o}$.

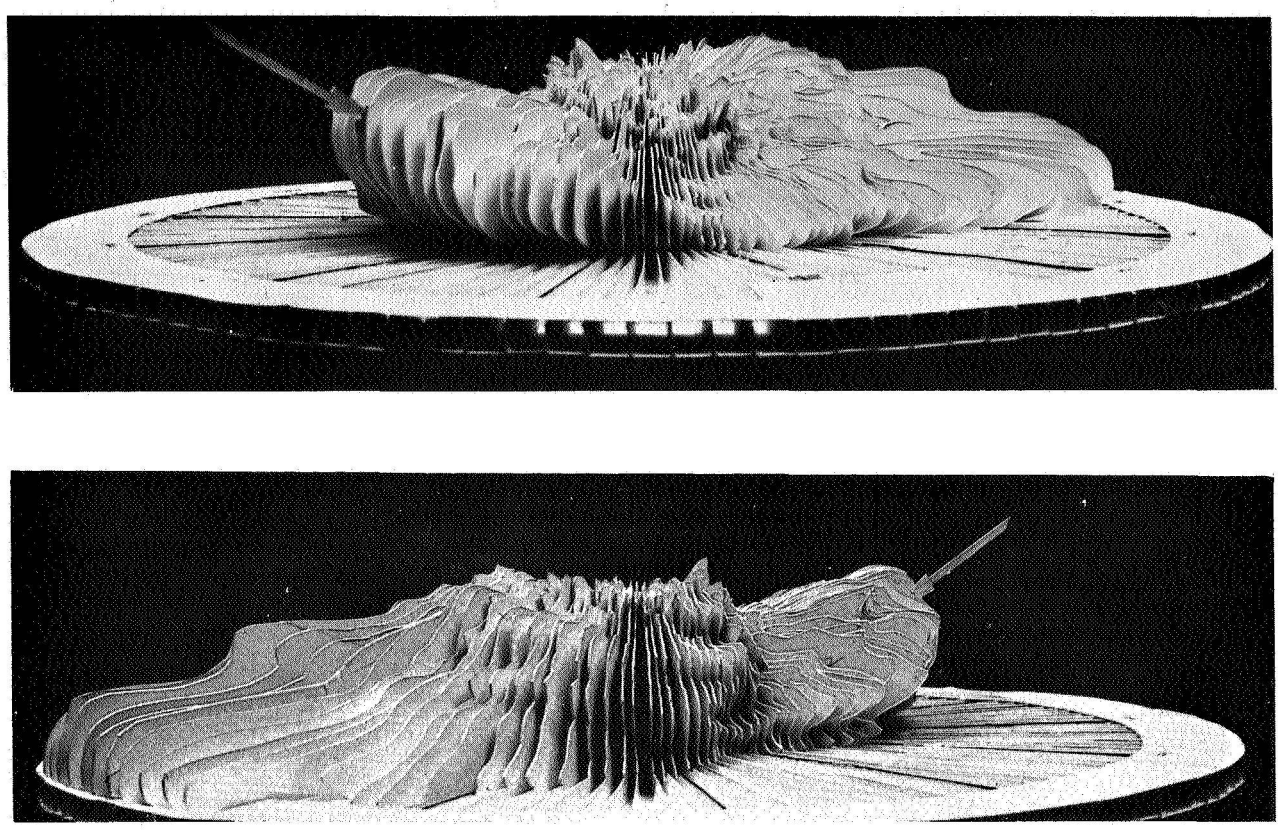

Figure 15. Photos of model of 0855-0909 CST bi-directional reflectance pattern $\theta_o = 68.3$

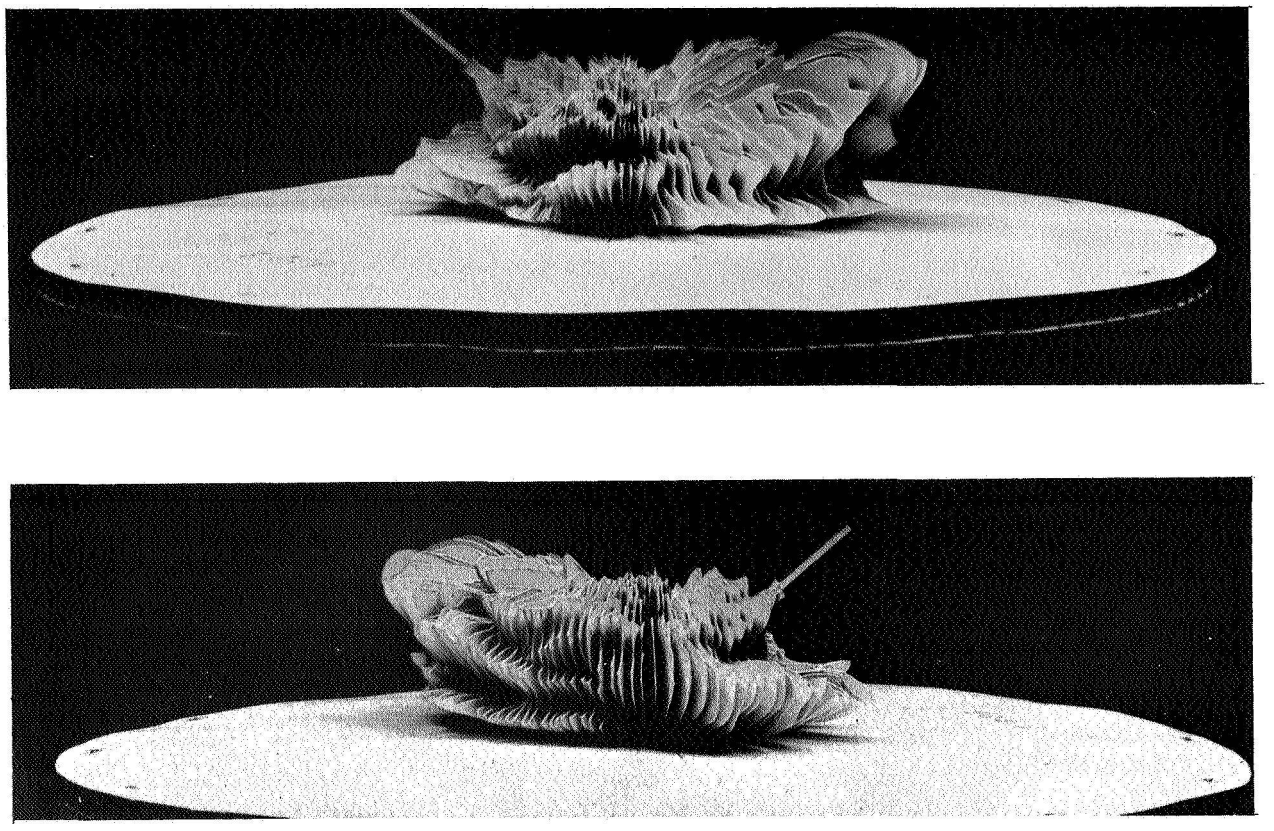

Figure 16. Photos of model of 1109-1116 CST bi-directional reflectance pattern. θ_o = 50.5-50.0°